APL Photonics

Versatile silicon microwave photonic spectral shaper

Cite as: APL Photonics **6**, 036106 (2021); https://doi.org/10.1063/5.0033516
Submitted: 16 October 2020 . Accepted: 24 February 2021 . Published Online: 11 March 2021

Xin Guo, Yang Liu, Tangman Yin, Blair Morrison, Mattia Pagani, Okky Daulay, Wim Bogaerts, Benjamin J. Eggleton, Alvaro Casas-Bedoya, and David Marpaung

Versatile silicon microwave photonic spectral shaper

Cite as: APL Photon. 6, 036106 (2021); doi: 10.1063/5.0033516
Submitted: 16 October 2020 • Accepted: 24 February 2021 •
Published Online: 11 March 2021

Xin Guo,[1,2,3] Yang Liu,[1,3] Tangman Yin,[1,3] Blair Morrison,[1,3] Mattia Pagani,[1,3] Okky Daulay,[2] Wim Bogaerts,[4] Benjamin J. Eggleton,[1,3] Alvaro Casas-Bedoya,[1,3,a)] and David Marpaung[2,a)]

AFFILIATIONS

[1] Institute of Photonics and Optical Science (IPOS), School of Physics, The University of Sydney, NSW 2006, Australia
[2] Nonlinear Nanophotonics group-LPNO, MESA+ Institute for Nanotechnology, University of Twente, Enschede, The Netherlands
[3] The University of Sydney Nano Institute (Sydney Nano), The University of Sydney, NSW 2006, Australia
[4] Ghent University - IMEC, Department of Information Technology, Photonics Research Group Technologiepark-Zwijnaarde 126, 9052 Gent, Belgium

[a)] **Authors to whom correspondence should be addressed:** alvaro.casasbedoya@sydney.edu.au and david.marpaung@utwente.nl

ABSTRACT

Optical modulation plays arguably the utmost important role in microwave photonic (MWP) systems. Precise synthesis of modulated optical spectra dictates virtually all aspects of MWP system quality including loss, noise figure, linearity, and types of functionalities that can be executed. However, for such a critical function, the versatility to generate and transform analog optical modulation is severely lacking, blocking the pathways to truly unique MWP functions including ultra-linear links and low-loss high rejection filters. Here, we demonstrate a versatile radiofrequency (RF) photonic spectral shaper integrated in a silicon photonic circuit. The spectral shaper controls the two modulation bands generated from an electro-optic modulation process in their relative amplitude and phase, offering an enhanced versatility for microwave-photonic modulation applications. Using the spectral shaper, we show electrically tailorable modulation transformations. Furthermore, we show a series of unprecedented RF filtering experiments through monolithic integration of the spectral shaper with a network of reconfigurable ring resonators.

I. INTRODUCTION

In a canonical microwave photonic (MWP) system,[1,2] radiofrequency (RF) signals are shaped and manipulated using optical techniques and components for wider processing bandwidth and advanced functionalities, which include tunable filtering,[3,4] microwave beamsteering,[5] tailored RF waveform generation,[6] and RF spectrum analysis.[7] Optical modulation, as the step to translate an RF signal into the optical domain, is the most critical step in all of these systems with its significance going beyond simple encoding of the RF information onto the optical carrier. In the frequency domain, optical modulation synthesizes a spectrum consisting of an optical carrier and two first-order RF-modulated sidebands. The phase and amplitude relations between these spectral components are essential in determining the types of functionalities that can be achieved in MWP systems. Upon photodetection, the mixing products of the optical carrier and the RF sidebands will interfere at the RFs and dictate the phase and amplitude of the output RF signals. In these views, versatile control and shaping of RF modulated spectral components are critical to determining the overall performance and characteristics of a microwave photonic system.

Versatile spectral shaping has been widely explored in the context of optical communications using a liquid crystal-on-silicon (LCoS)-based signal processor that can be reconfigured to perform wavelength selective switching[8] and optical pulse shaping.[9] Such a photonic signal processor, also usually termed the "waveshaper," has also been implemented in various microwave photonic

applications including tunable true time delay beamforming[10] and tunable notch filtering.[11] However, despite their versatility, chip integration of LCoS waveshapers remains a challenge. Several efforts have been proposed to miniaturize the signal shaper through integration of arrayed waveguide gratings in a doped-silica platform.[12,13] Another challenge to overcome in the chip integration of waveshapers is achieving high spectral resolution that is currently of the order of 0.8 GHz.[12] Another approach for this demultiplexing is to use a waveguide ring resonator based demultiplexer in low loss materials such as silicon nitride.[14]

Implementation of a waveshaper-like versatile signal processor specifically for microwave photonics requires a different strategy. For a start, the recent proliferation of integrated microwave systems requires co-integration of the spectral shaper with larger libraries of components including optical modulators and photodetectors, as well as reprogrammable optical signal processor engines carrying out tasks such as filtering, true time delay, and phase shifting. In a more fundamental sense, the microwave photonic spectral shaper at its simplest implementation needs to process three main spectral components, the optical carrier and the first-order RF modulated sidebands, as opposed to a high count of spectral channels as in the case of traditional waveshapers. Such an implementation, allowing for full control of the phase and amplitude of the three main spectral components, will already allow for versatile modulation transformation. This is a highly desired functionality that can be challenging to implement in traditional optical modulator topologies. Phase or intensity modulators, for example, always create the optical carrier and RF sidebands with interrelated phases and amplitudes. Although the use of combination of phase and amplitude modulators, such as in the dual-parallel Mach–Zehnder modulators (DPMZMs), offers higher flexibility in synthesizing the modulated spectra, complete phase and amplitude control still cannot be achieved.[11] Recent results have shown that complete phase and amplitude control of an optical modulation spectrum can create opportunities for new and enhanced RF-photonic signal processing functions free from the performance trade-offs typically faced in RF photonic systems, including advanced RF photonic filters with minimal loss and maximal rejection[3,15,16] and linearized microwave photonic links.[17] Thus, a device that targets an entirely new level of freedom in synthesizing a modulated spectrum will thus be significant to unlock unexplored degrees of freedom in microwave photonics.

II. PRINCIPLE OF OPERATION

In this work, we present a circuit to synthesize and shape arbitrary RF photonic spectra using an all-integrated silicon photonic chip.[18] A modulated optical spectrum at the input of the circuit will be transformed into an output spectrum with spectral components (optical carrier and RF sidebands) entirely independent in the phase and amplitude, essentially performing a universal modulation transformation. The operation of this circuit is markedly different compared to prior techniques specifically aimed at phase-to-intensity modulation (PM–IM) conversion.[19,20] Such techniques rely solely on the phase rotation of the optical carrier and, thus, can only switch between PM and IM.

The operational principle of the spectrum shaping circuit is depicted in Fig. 1. The two output ports of the spectral de-interleaver consist of completed complementary spectra. To achieve proper spectral shaping and modulation transformation, one sideband of an input RF photonic spectrum is spatially isolated from the optical carrier and the remaining sideband via a spectral de-interleaver. The phase and amplitude of the isolated sideband can thus be further manipulated through an in-line phase shifter and a tunable attenuator, respectively. In principle, combining this tailored sideband with the rest of the spectrum will complete the modulation transformation process.

This versatile spectral shaping process can further be combined with complementary signal processing intended for activating RF photonic functionalities. For example, a tunable filter network can be placed in the path of the optical carrier and the un-isolated sideband prior to recombination. Proper tailoring of the RF modulated spectrum in combination with complex optical filtering provided by the filter network will lead to advanced high-performance RF filters at the photodetector output. The operation of the spectrum shaping circuit can be verified through inspection of optical spectra at

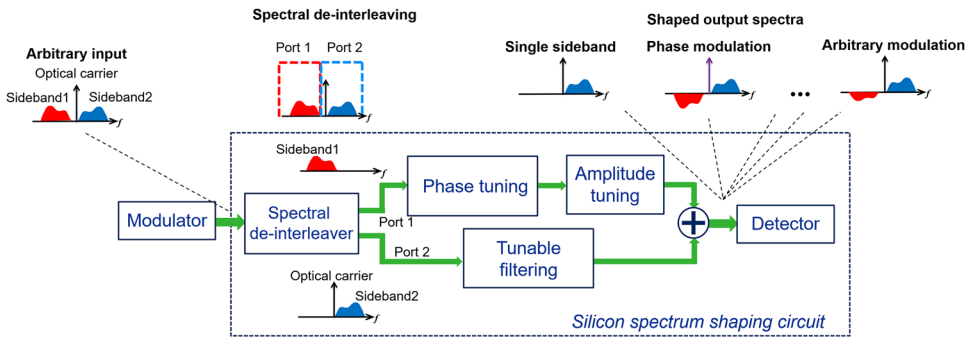

FIG. 1. Principle of operation of the spectrum shaping circuit. The spectral de-interleaver is used to isolate a sideband from the rest of the RF-modulated optical spectrum. A cascade of a tunable phase shifter and an attenuator is used to manipulate the phase and amplitude of the isolated sideband. Recombination with the unprocessed spectral components yields a versatile spectrum shaping, producing various modulation formats such as single-sideband modulation, phase modulation, and advanced arbitrary modulation. Moreover, the combination of a tunable filtering element with the spectrum shaping circuit leads to advanced reconfigurable RF photonic filtering functionalities.

various tapped output ports prior to photodetection, as well as measuring the RF mixing products of the optical carrier and the two sidebands at the photodetector output.

III. RESULTS

A. Circuit implementation

The implementation of the spectrum shaping circuit is illustrated in Fig. 2. We realize the spectral de-interleaver using a Mach–Zehnder interferometer (MZI) loaded with three ring resonators (MZI+3 rings) topology.[21] The two outputs of the de-interleaver exhibit square-shaped, flat-top complementary filters. The de-interleaver outputs containing the isolated sideband are routed to a cascade of a thermo-optic phase shifter and a tunable coupler implemented as a balanced MZI, for independent phase and amplitude tailoring. The complementary output of the de-interleaver carries the optical carrier and the un-isolated sideband and is routed to a cascade of all-pass and add–drop ring resonators. These rings are used to implement tunable filtering on the un-isolated sideband. The two waveguide paths are then recombined in a 3-dB coupler to synthesize a new spectrum with designer phase and amplitude relations between its spectral components. One of the two outputs of the 3-dB coupler is sent to an on-chip photodetector and the other routed off-chip through a grating coupler.

The spectrum shaping circuit was fabricated in IMEC's silicon photonic iSiPP25G process through the Europractice multi-project wafer service. All key components in the circuit including the phase shifters, tunable couplers, and de-interleaver were fully tunable through thermo-optic tuning. The spectrum shaping circuit was designed to flexibly work either with an external modulator or with an on-chip Mach–Zehnder modulator (see Appendix A for the details of the device design and fabrication). Due to limited bandwidth, the fabricated on-chip modulator was not used in any of the experiments. All measurements were performed using external modulators. Figure 2(b) shows the picture of our silicon chip, and the circuit layout is given in Fig. 2(c).

We characterized the individual components in the circuit and compared the measurement results with our model results, developed using the z-transform approach, as described in Section 1 of the supplementary material. The transmission spectrum of the de-interleaver is depicted in Fig. 3(a). Optimized tuning of the heaters on the circuit leads to a de-interleaver with complementary outputs with 30 GHz-wide pass and stop bands and a rejection of more than 20 dB. The filtering response of the all-pass ring resonator and add–drop ring resonator of the followed ring network circuits is shown in Figs. 3(b) and 3(c), respectively. The free-spectral range (FSR) of the rings is 0.4 nm (50 GHz). Comparing the measured responses with simulation results, we extract the maximum loaded Q-factors of the all-pass and add–drop rings to be 120 000. At critical coupling, the Q-factor and finesse of the all-pass ring were 68 000 and 17.6, respectively [Fig. 3(b)]. We measured the fiber-to-fiber optical loss of 20 dB from our silicon chip, which includes the coupling loss (around 5 dB per facet), propagation loss, and loss induced by couplers in the circuit.

B. Modulation transformation experiments

To demonstrate the versatility of our approach, we controlled our circuit to synthesize various RF modulation schemes from a conventional phase or intensity modulation input. In these series of experiments, described in detail in Appendix B, we used the on-chip photodetector in combination with external electro-optic modulators (as illustrated in Fig. 4(a)) to ensure high bandwidth operation. The on-chip modulator, on the other hand, exhibited limited bandwidth of 11 GHz as compared to the de-interleaver bandwidth (30 GHz). Moreover, we observed high internal RF crosstalk in our chip (see Section 4 of the supplementary material for details).

In the first experiment, an intensity modulated signal is sent to the circuit and the optical phase shifter is used to modify the phase of

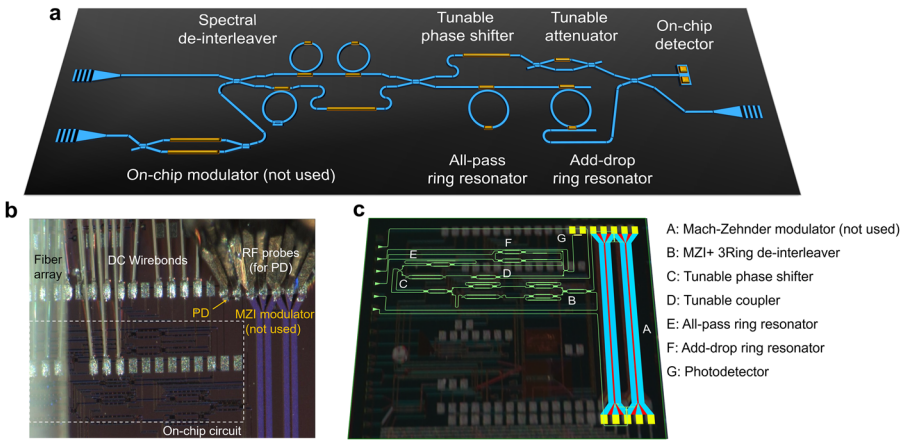

FIG. 2. Implementation of the spectrum shaping circuit in a silicon chip. (a) Artistic representation of the silicon spectrum shaping circuit showing the active components (a modulator and a photodetector) and passive optical circuit containing the Mach–Zehnder interferometer loaded with three ring resonators (MZI+3 rings) as the spectral de-interleaver. A cascade of all-pass and add–drop ring resonators is used to implement RF photonic filtering. (b) Picture of the silicon ship. (c) Circuit layout of the silicon chip overlaid on the photograph of the chip. Due to a limited bandwidth of 11 GHz, the fabricated on-chip modulator was not used in the experiments. All measurements were performed using external modulators.

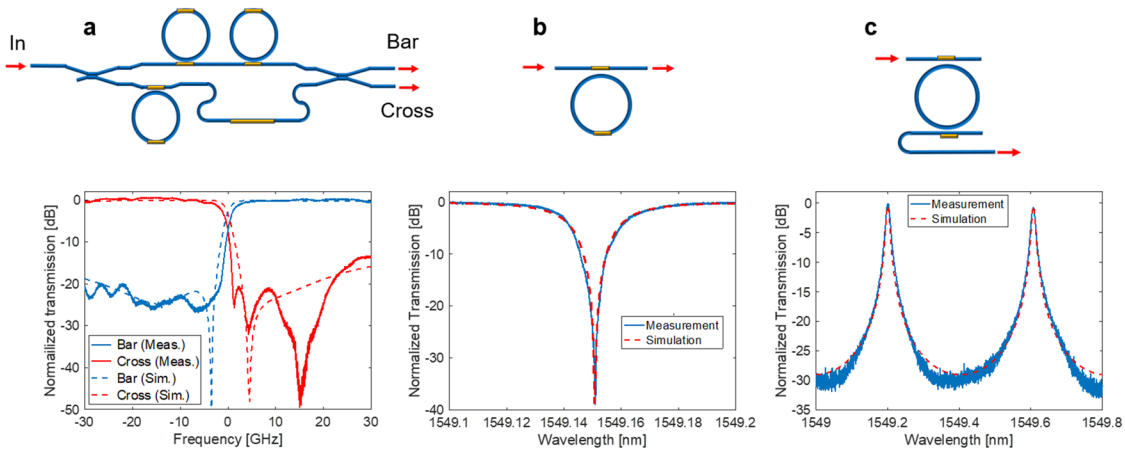

FIG. 3. Characterization of the individual components in the circuit. (a) Transmission spectrum of the de-interleaver revealing 30 GHz channel bandwidth and more than 20 dB extinction. (b) Measured (solid line) and modeled (dashed line) filtering responses of an all-pass ring. (c) Measured (solid line) and simulated (dashed line) filtering responses of an add–drop ring at the drop port.

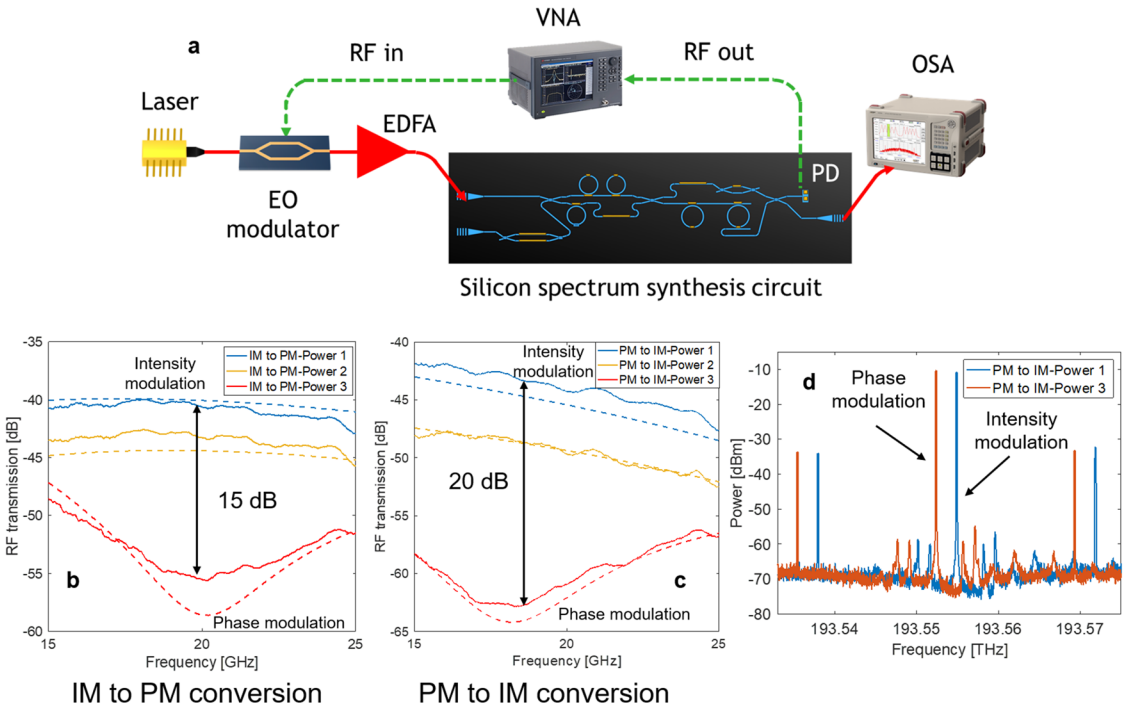

FIG. 4. Setup and results of modulation transformation experiments. (a) Schematic of the experimental setup used to characterize RF modulation transformation and RF photonic filtering. EDFA: erbium-doped fiber amplifier; PD: photodetector; VNA: RF vector network analyzer; OSA: optical spectrum analyzer. (b) Results of the intensity to phase modulation (IM to PM) conversion experiment showing 15 dB extinction, in which the intensity modulation produces a high RF link gain, while the phase modulation produces a significantly reduced RF link gain due to the destructive interference of out-of-phase sidebands. We gradually tuned the phase shifter (adding more power) to realize this conversion, where values of IM to PM power 1, 2, 3 are 21.4 mW, 38.0 mW, and 114.2 mW. (c) Results of the phase to intensity modulation (PM to IM) conversion experiment exhibiting 20 dB extinction, where the values of PM to IM power 1, 2, 3 are 28.8 mW, 51.0 mW, and 65.3 mW. (d) Synthesized optical spectra with intensity and phase modulation in the PM to IM conversion experiment reveal similar features in the amplitude spectrum, proving that the modulation format transformation was due to phase rotation of the sideband.

the isolated sideband to synthesize phase modulation from an intensity modulation input (IM–PM conversion). When both sidebands are in-phase, the measured RF transmission is high, as shown in the blue trace of Fig. 4(b). We then tuned the circuit to rotate the phase of the isolated sideband and synthesize phase modulation. When the sidebands are out-of-phase, the RF transmission is minimized, indicating phase modulation [red trace in Fig. 4(b)]. The extinction of the IM–PM conversion was 15 dB. We then replaced the intensity modulator with a phase modulator and repeated the experiments whose results are depicted in Fig. 4(c). In this experiment, the phase modulation input was transformed to the intensity modulation output. To show the continuous tunability of the modulation transformation, we show the intermediate state between PM and IM, as shown by the yellow traces in Figs. 4(b) and 4(c). For both experiments, we achieved modulation transformation with a 10 GHz bandwidth. An RF transmission extinction up to 15 dB can be achieved in these experiments solely by electrical tuning of the phase shifter following the bar port of the de-interleaver. The bandwidth and the extinction of the modulation transformation are mainly limited by the roll-off and the dispersion of the MZI+3 ring de-interleaver, in particular at the transition band. The details of the simulations and the parameters of the experiments can be found in Section 2 of the supplementary material.

We verified that the modulation transformation was achieved purely from phase tuning effects by inspecting the optical spectra of the corresponding RF traces. Both traces in Fig. 4(b), with either high or low RF transmission, were showing practically identical optical spectra as shown in Fig. 4(d). This is expected because the recorded optical spectra carry no information about the relative phase difference between the sidebands and the optical carrier. By comparing the datasets in Figs. 4(b)–4(d), one can conclude that the large extinction of RF transmission solely comes from the phase rotation effect that leads to either fully constructive or destructive interference between the mixing products of the carrier and the RF sidebands. It should be noted that, in the experiment, the central frequency of the laser needs to be slightly adjusted due to the drift in central frequencies of the de-interleaver passbands, which was attributed to the thermal crosstalk in the circuit. With further characterization, this could be compensated by adaptive control of the thermal tuners.[22]

C. Advanced RF filtering experiments

Reconfigurable modulation transformations will enable various RF photonic filtering schemes[23–25] in a single chip-scale device using the simplest modulator configuration such as a phase modulator. Prior to this work, achieving such a versatile transformation would have been challenging especially because silicon photonic modulators are known to exhibit not just phase modulation but also spurious amplitude modulation. Here, we demonstrated three distinct RF photonic filtering topologies that would require very different kinds of input modulations to the photonic filtering elements. Using our silicon photonic circuit, we shaped RF photonic spectra from a common intensity modulator input to match the subsequent filtering function provided by on-chip resonator networks and show conventional single sideband (SSB) bandpass and bandstop filters as well as a high-extinction RF-interference notch filter in a single reconfigurable device.

Figure 5 depicts the experimental schematic and the optical or RF spectrum at each stage of the three RF photonic filter topologies demonstrated here. We first configured the modulation transformer to synthesize single sideband (SSB) modulation by activating the tunable coupler to completely block the isolated sideband [Fig. 5(a)]. We sent the remaining carrier and sideband to an all-pass ring resonator to form an SSB RF photonic notch filter. The resulting RF filter response is shown as a dashed line in Fig. 5(d). The rejection of the RF notch filter is proportional to rejection in the optical domain, which was set to 7 dB.

Next, we reconfigured the circuit to show a complex phase cancellation filter[26] that can amplify the shallow rejection of the all-pass ring to a much higher extinction. This requires the modulation transformer to synthesize a new spectrum with unequal-amplitude and anti-phase sidebands [Fig. 5(b)]. Here, the isolated sideband was attenuated by 7 dB and rotated in phase to exhibit the π phase shift with respect to the un-isolated sideband. We then sent this spectrum to the all-pass ring. At the notch frequency, the amplitudes of the two sidebands are equal, but they are opposite in phase, which, upon photodetection, will form an ultra-high rejection RF notch filter of 38 dB [solid line in Fig. 5(d)]. Data for the central frequency tuning of the notch filters can be found in Section 5 of the supplementary material.

In the third filtering experiment, we demonstrate bandpass filtering using an add–drop ring resonator [Fig. 5(c)]. The challenge in this filtering experiment is that the passband of the ring is too narrow to pass both the optical carrier and a tunable-frequency sideband, so forming a tunable RF photonic bandpass filter without precise carrier re-insertion is, in fact, impossible. We mitigate this limitation using our modulation transformer. First, we synthesize an SSB + carrier spectrum at the input. We configured the modulation transformer to separate the carrier and the sideband, where the latter is being passed to the add–drop ring to be filtered. The 3-dB coupler re-combined the carrier and the processed sideband to form a true SSB RF photonic bandpass filter. We then tuned the resonance frequency of the add–drop ring, resulting in a tuned central frequency of the RF bandpass filter, as depicted in Fig. 5(e). The observed variation of the bandpass filter magnitude response seen in Fig. 5(e) might result from the thermal crosstalk in the silicon chip. When the on-chip heater that controls the add–drop ring resonance frequency was tuned, thermal crosstalk leads to slight variations of the coupling states between the ring and bus waveguides. These slight variations manifest as changes in the passband response of the microwave photonic filter.

The experiment results depicted in Fig. 5 highlight the versatility of the spectral shaper in conjunction with a filtering element. Nevertheless, for the carrier re-insertion experiment presented in Figs. 5(c) and 5(e), an external SSB modulator was required. Ideally, the input SSB + carrier spectrum should also be synthesized in the modulation transformer. However, the modulation transformer topology presented in this work only allows two complementary output spectra to be synthesized. This is not sufficient to carry out both tasks of the modulation transformation to SSB + carrier and the optical carrier re-insertion required in the third filtering experiment. In this case, modulation transformation with three complementary outputs is required. Such a topology can be implemented using two cascaded de-interleavers.

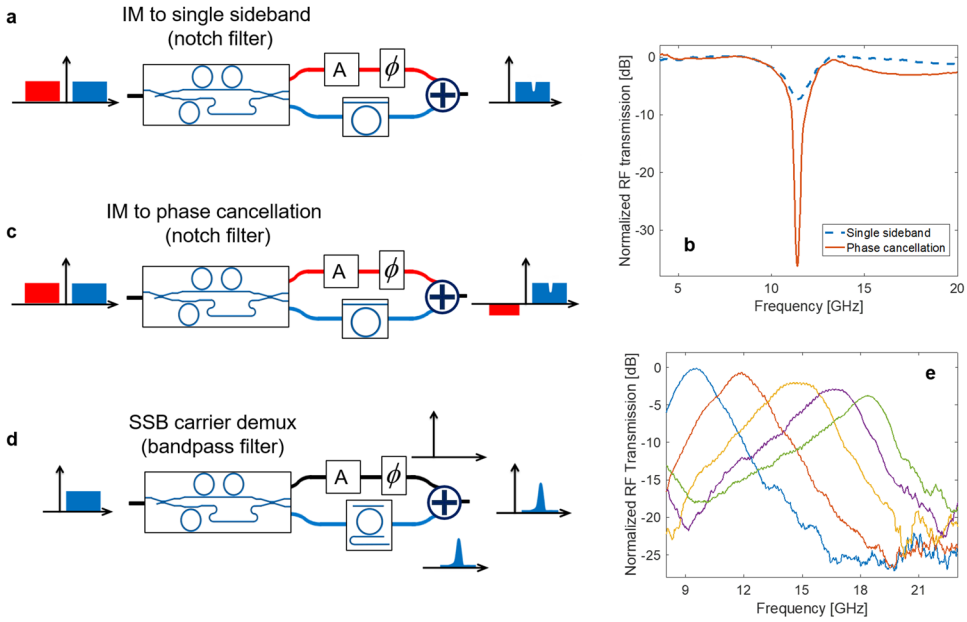

FIG. 5. Configurations and results of RF filtering experiments. (a) Single sideband notch filter experiment where the spectrum shaping circuit was used to remove the lower RF sideband. (b) Phase cancellation notch filter, where the circuit was used to synthesize RF sidebands with unbalanced amplitude and opposite phase. (c) A bandpass filter where the circuit was used as a carrier re-insertion network. (d) Comparison of RF notch filter responses from the single-sideband scheme in (a) and the phase cancellation filter in (b). With the same optical filter response, the single-sideband filter shows a shallow response (blue dashed-trace), while the phase cancellation filter exhibits a deeper rejection enhanced by 30 dB (red solid trace). (e) Measured central frequency-tuned RF responses of the bandpass filter shown in (c). The tunability is realized by gradually increasing the power of the heater (corresponding to the curves from left to right) that controls the resonance of the drop ring.

IV. DISCUSSION

The concept of RF photonic spectrum manipulation presented here can be extended beyond modulation transformation and filtering. Full phase and amplitude control of the optical carrier and RF sidebands up to higher order can be used to linearize RF photonic links as has been recently demonstrated,[17,27–29] to create tailorable RF waveforms,[6,30] or to improve the gain and noise figure of microwave photonic systems.[22,31,32] Independent control of optical carrier and sideband amplitudes in the circuit can be used to optimize the modulation index and power ratio of these spectral components and to emulate low biasing of a Mach–Zehnder modulator.[33]

The work presented here is a fundamental demonstration of RF photonic spectrum shaping and modulation transformation principles, but it is currently limited by realizable technologies. Two essential building blocks to execute modulation transformation proposed here, namely, the spatial separation of individual spectral components and the independent phase and amplitude tailoring, are still beset by non-idealities in the complex transfer functions of the de-interleaver, the phase shifter, and the tunable coupler. For example, the roll-off in the magnitude response of the de-interleaver limits the lowest RFs that can be processed. This roll-off is a very sensitive function of the waveguide propagation loss, which amounts to 1.2 dB/cm in our demonstration. Shifting these functions to lower loss platforms such as silicon nitride will lead to considerable improvements in the filter sharpness. On the other hand, the nonlinear phase response at the transition bands of the de-interleaver restricts the achievable modulation transformation bandwidth. This is a more fundamental limitation that cannot simply be solved by reducing waveguide losses. Alternative de-interleaver design with more linear phase response, such as using cascaded Mach–Zehnder interferometers (MZIs),[34] can be considered.

Broadband and independent phase and amplitude tailoring is essential to achieve tractable modulation transformation. Present implementation with the tunable phase shifter and MZI-based tunable coupler leads to limited bandwidth and interrelated phase and amplitude tuning. When tuned, the tunable coupler exhibits parasitic phase rotation that always needs to be compensated by tuning the phase shifter (see Section 1 of the supplementary material). Bandwidth limitation of spectrum transformation also comes from the optical path-length difference between the de-interleaved spectra. A thermo-optic phase shifter is not suitable to compensate this path-length difference. Instead, a tunable optical delay line is required.

Finally, RF metrics are important aspects of microwave photonics. As we point out in this paper, these metrics are directly related to the control of optical modulated spectra that can be synthesized by the modulators and spectral shapers. In this work, we focus on the versatility of controlling these spectra and its impact on the formation of the tunable microwave photonic filter as an example. We did not optimize for the RF metrics in this particular work. To do so, we will require spectral shaping implementation in a low

loss platform in combination with techniques to mitigate RF losses, including increasing input optical power.

V. CONCLUSION

In summary, we demonstrated an RF photonic spectral shaper with both passive and active components on a monolithic silicon photonic circuit. The circuit allows for independent tailoring of the phase and amplitude of the optical carrier and RF sidebands leading to the demonstration of versatile RF photonic modulation transformation. With this novel concept, we demonstrated three distinct kinds of RF photonic filters using a simple intensity modulator, showing the potential of the concept for advanced microwave photonic functions. This work will serve as the basis of further RF photonic noise, dynamic range, and filter optimizations and stabilization through modulation spectral shaping and transformation.

SUPPLEMENTARY MATERIAL

See the supplementary material for the supporting content.

ACKNOWLEDGMENTS

The authors acknowledge the facilities as well as the scientific and technical assistance of the Research and Prototype Foundry Core Research Facility at the University of Sydney, part of the Australian National Fabrication Facility. They acknowledge technical assistance from C. Cantaloube and use of facilities provided by Microsoft Quantum, Sydney.

The authors acknowledge funding from the Australian Research Council (ARC) through ARC DECRA (Grant No. DE150101535), the Laureate Fellowship (Grant No. FL120100029), and the Center of Excellence CUDOS (Grant No. CE110001018), and the Netherlands Organisation for Scientific Research (NWO) Vidi (15702) and Start Up (740.018.021).

APPENDIX A: DETAILS OF DEVICE DESIGN AND FABRICATION

The silicon chip was designed with the IPKISS parametric design framework[35] and fabricated in IMEC's iSiPP25G process[36] through the Europractice multi-project wafer service. The key building blocks are implemented as SOI nanowires with 220 × 450 nm^2 dimension. The optical waveguide loss is 1.2 dB/cm. All components are tunable using thermo-optic tuning. To get the device with full reconfiguration capability and to compensate for any fabrication imperfection, we designed the 3-dB couplers of the de-interleaver and the waveguide-ring couplers as a tunable symmetric MZI coupler. The modulator is a 1.5 mm long Mach–Zehnder modulator with depletion-type phase shifters with 11 GHz RF bandwidth and the photodetector is a 40 GHz Ge-PD with the responsivity of 0.8 A/W, both being taken from the provided iSiPP25G design kit. The de-interleaver was designed to have a passband width of 30 GHz and peak rejection of 30 GHz. The all-pass and add–drop rings both have a free spectral range (FSR) of 50 GHz. The maximum quality factor of the all-pass and the add–drop rings was 120 000. The silicon chip was wire bonded locally onto a bespoke PCB for ease of experiments. The optical signal is coupled in and out of the chip using grating couplers, with a 3-dB loss per coupler.

APPENDIX B: DETAILS OF THE EXPERIMENTAL SETUP

In the experiments, we used a tunable diode laser (Yenista TUNICS T100S-HP) with 0 dBm of output power, connected to an intensity modulator (Thorlabs, LN05S-FC) or a phase modulator (Thorlabs, LN27S-FC). The output of the modulator is connected to an EDFA (Amonics) with the maximum output power of 19.1 dBm. The chip is mounted on a vertically coupled computer controlled fiber stage (Maple Leaf Photonics); the fiber array contains 19 output ports with an interval of 127 μm. For measurements of the de-interleaver phase response, an external photodetector (Finisar, XPDV2120RA-VF-FP) was used, while the rest of the measurements were done using the on-chip photodetector. Optical spectrum analysis was performed using a high-resolution spectrum analyzer (Apex, AP2083A). For the RF transmission measurement, a frequency-swept RF signal with 0 dBm power was supplied from and measured on a 10 MHz–43.5 GHz vector network analyzer (Agilent, PNA 5224A).

DATA AVAILABILITY

The data that support the findings of this study are available from the corresponding authors upon reasonable request.

REFERENCES

[1] J. Capmany and D. Novak, "Microwave photonics combines two worlds," Nat. Photonics **1**, 319–330 (2007).

[2] D. Marpaung, J. Yao, and J. Capmany, "Integrated microwave photonics," Nat. Photonics **13**, 80–90 (2019).

[3] D. Marpaung, B. Morrison, M. Pagani, R. Pant, D.-Y. Choi, B. Luther-Davies, S. J. Madden, and B. J. Eggleton, "Low-power, chip-based stimulated Brillouin scattering microwave photonic filter with ultrahigh selectivity," Optica **2**, 76–83 (2015).

[4] X. Xu, M. Tan, J. Wu, T. G. Nguyen, S. T. Chu, B. E. Little, R. Morandotti, A. Mitchell, and D. J. Moss, "High performance RF filters via bandwidth scaling with Kerr micro-combs," APL Photonics **4**, 026102 (2019).

[5] V. C. Duarte, J. G. Prata, C. F. Ribeiro, R. N. Nogueira, G. Winzer, L. Zimmermann, R. Walker, S. Clements, M. Filipowicz, M. Napierała, and T. Nasiłowski, "Modular coherent photonic-aided payload receiver for communications satellites," Nat. Commun. **10**, 1984 (2019).

[6] J. Wang, H. Shen, L. Fan, R. Wu, B. Niu, L. T. Varghese, Y. Xuan, D. E. Leaird, X. Wang, F. Gan, A. M. Weiner, and M. Qi, "Reconfigurable radio-frequency arbitrary waveforms synthesized in a silicon photonic chip," Nat. Commun. **6**, 5957 (2015).

[7] M. Burla, X. Wang, M. Li, L. Chrostowski, and J. Azaña, "Wideband dynamic microwave frequency identification system using a low-power ultracompact silicon photonic chip," Nat. Commun. **7**, 13004 (2016).

[8] M. A. F. Roelens, S. Frisken, J. A. Bolger, D. Abakoumov, G. Baxter, S. Poole, and B. J. Eggleton, "Dispersion trimming in a reconfigurable wavelength selective switch," J. Lightwave Technol. **26**, 73–78 (2008).

[9] A. M. Eggleton, "Ultrafast optical pulse shaping: A tutorial review," Opt. Commun. **284**, 3669–3692 (2011).

[10] X. Yi, T. X. H. Huang, and R. A. Minasian, "Photonic beamforming based on programmable phase shifters with amplitude and phase control," IEEE Photonics Technol. Lett. **23**, 1286–1288 (2011).

[11] S. Shahnia, M. Pagani, B. Morrison, B. J. Eggleton, and D. Marpaung, "Independent manipulation of the phase and amplitude of optical sidebands in a highly-stable RF photonic filter," Opt. Express **23**, 23278–23286 (2015).

[12] R. Rudnick, A. Tolmachev, D. Sinefeld, O. Golani, S. Ben-Ezra, M. Nazarathy, and D. M. Marom, "Sub-GHz resolution photonic spectral processor and its system Applications," J. Lightwave Technol. **35**, 2218–2226 (2017).

[13]K. Takiguchi, "'Integrated-optic spectrum synthesis circuit for manipulating 64 frequency components,' next-generation optical communication: Components," Sub-Systems, Systems IX **11309**, 113090F (2020).
[14]L. Zhuang, C. Zhu, B. Corcoran, M. Burla, C. G. H. Roeloffzen, A. Leinse, J. Schröder, and A. J. Lowery, "Sub-GHz-resolution C-band Nyquist-filtering interleaver on a high-index-contrast photonic integrated circuit," Opt. Express **24**, 5715–5727 (2016).
[15]A. Casas-Bedoya, B. Morrison, M. Pagani, D. Marpaung, and B. J. Eggleton, "Tunable narrowband microwave photonic filter created by stimulated Brillouin scattering from a silicon nanowire," Opt. Lett. **40**, 4154–4157 (2015).
[16]L. Zhuang, M. Burla, C. Taddei, C. G. H. Roeloffzen, M. Hoekman, A. Leinse, K.-J. Boller, and A. J. Lowery, "Integrated microwave photonic splitter with reconfigurable amplitude, phase, and delay offsets," Opt. Lett. **40**, 5618–5621 (2015).
[17]G. Liu, O. Daulay, Q. Tan, H. Yu, and D. Marpaung, "Linearized phase modulated microwave photonic link based on integrated ring resonators," Opt. Express **28**, 38603–38615 (2020).
[18]X. Guo, T. Yin, Y. Liu, B. Morrison, C. Cantaloube, W. Bogaerts, B. J. Eggleton. D. Marpaung, and A. C. Bedoya. "All-integrated universal RF photonic spectral shaper," in *Asia Communications and Photonics Conference (ACP)* (OSA, 2019).
[19]L. Zhuang, M. Hoekman, C. Taddei, A. Leinse, R. G. Heideman, A. Hulzinga, J. Verpoorte, R. M. Oldenbeuving, P. W. L. van Dijk, K.-J. Boller, and C. G. H. Roeloffzen, "On-chip microwave photonic beamformer circuits operating with phase modulation and direct detection," Opt. Express **22**, 17079–17091 (2014).
[20]W. Li, N. Zhu, L. X. Wang, and H. Wang, "Broadband phase-to-intensity modulation conversion for microwave photonics processing using Brillouin-assisted carrier phase shift," J. Light. Technol. **29**, 3616–3621 (2011).
[21]P. Daniel, I. Gasulla, L. Crudgington, D. J. Thomson, A. Z. Khokhar, K. Li, W. Cao, G. Z. Mashanovich, and J. Capmany, "Multipurpose silicon photonics signal processor core," Nat. Commun. **8**, 1925 (2017).
[22]M. Milanizadeh, S. Ahmadi, M. Petrini, D. Aguiar, R. Mazzanti, F. Zanetto, E. Guglielmi, M. Sampietro, F. Morichetti, and A. Melloni, "Control and calibration recipes for photonic integrated circuits," IEEE J. Sel. Top. Quantum Electron. **26**, 1–10 (2020).
[23]Y. Liu, J. Hotten, A. Choudhary, B. J. Eggleton, and D. Marpaung, "All-optimized integrated RF photonic notch filter," Opt. Lett. **42**, 4631–4634 (2017).
[24]Y. Liu, D. Marpaung, A. Choudhary, J. Hotten, and B. J. Eggleton, "Link performance optimization of chip-based Si_3N_4 microwave photonic filters," J. Light Technol. **36**, 4361–4370 (2018).
[25]Y. Liu, A. Choudhary, D. Marpaung, and B. J. Eggleton, "Integrated microwave photonic filters," Adv. Opt. Photonics **12**, 485–555 (2020).
[26]D. Marpaung, B. Morrison, R. Pant, C. Roeloffzen, A. Leinse, M. Hoekman, R. Heideman, and B. J. Eggleton, "Si_3N_4 ring resonator-based microwave photonic notch filter with an ultrahigh peak rejection," Opt. Express **21**, 23286–23294 (2013).
[27]R. Wu, T. Jiang, S. Yu, J. Shang, and W. Gu, "Multi-order nonlinear distortions analysis and suppression in phase modulation microwave photonics link," J. Light Technol. **37**, 5973–5981 (2019).
[28]D. Zhu, J. Chen, and S. Pan, "Linearized phase-modulated analog photonic link with the dispersion-induced power fading effect suppressed based on optical carrier band processing," Opt. Express **25**, 10397–10404 (2017).
[29]Z. Xie, S. Yu, S. Cai, W. Gu, and W. Gu, "Simultaneous improvements of gain and linearity in dispersion-tolerant phase-modulated analog photonic link," IEEE Photonics J. **9**, 1–12 (2017).
[30]Z. Zhu, Y. Liu, M. Merklein, Z. Zhang, D. Marpaung, and B. J. Eggleton, "Si_3N_4-chip-based versatile photonic RF waveform generator with a wide tuning range of repetition rate," Opt. Lett. **45**, 1370–1373 (2020).
[31]Y. Liu, D. Marpaung, A. Choudhary, and B. J. Eggleton, "Lossless and high-resolution RF photonic notch filter," Opt. Lett. **41**, 5306–5309 (2016).
[32]Z. Zhu, Y. Liu, M. Merklein, O. Daulay, D. Marpaung, and B. J. Eggleton, "Positive link gain microwave photonic bandpass filter using Si_3N_4-ring-enabled sideband filtering and carrier suppression," Opt. Express **27**, 31727–31740 (2019).
[33]O. Daulay, G. Liu, and D. Marpaung, "Microwave photonic notch filter with integrated phase-to-intensity modulation transformation and optical carrier suppression," Opt. Lett. **46**, 488–491 (2021).
[34]F. Horst, W. M. J. Green, S. Assefa, S. M. Shank, Y. A. Vlasov, and B. J. Offrein, "Cascaded Mach-Zehnder wavelength filters in silicon photonics for low loss and flat pass-band WDM (de-) multiplexing," Opt. Express **21**, 11652–11658 (2013).
[35]W. Bogaerts, M. Fiers, M. Sivilotti, and P. Dumon, "The IPKISS photonic design framework," in *Optical Fiber Communications Conference and Exposition (OFC)* (OSA, 2016).
[36]M. Pantouvaki, S. A. Srinivasan, Y. Ban, P. De Heyn, P. Verheyen, G. Lepage, H. Chen, J. De Coster, N. Golshani, S. Balakrishnan, P. Absil, and J. Van Campenhout, "Active components for 50 Gb/s NRZ-OOK optical interconnects in a silicon photonics platform," J. Light Technol. **35**, 631–638 (2017).